ACS APPLIED MATERIALS & INTERFACES

www.acsami.org

Research Article

Tailoring Solvation Solvent in Localized High-Concentration Electrolytes for Lithium||Sulfurized Polyacrylonitrile

Ju-Myung Kim, Peiyuan Gao, Qiushi Miao, Qian Zhao, Muhammad Mominur Rahman, Ping Chen, Xin Zhang, Enyuan Hu, Ping Liu, Ji-Guang Zhang,* and Wu Xu*

Cite This: *ACS Appl. Mater. Interfaces* 2024, 16, 20618−20625

Read Online

ACCESS | Metrics & More | Article Recommendations | Supporting Information

ABSTRACT: Sulfurized polyacrylonitrile (SPAN) is a promising cathode material for lithium−sulfur (Li−S) batteries due to its significantly reduced polysulfide (PS) dissolution compared to that of elemental S cathodes. Although conventional carbonate-based electrolytes are stable with SPAN electrodes, they are unstable with Li metal anodes. Recently, localized high-concentration electrolytes (LHCEs) have been developed to improve the stability of Li anodes. Here, we report a new strategy to further improve the performance of Li||SPAN batteries by replacing the conventional solvating solvent 1,2-dimethoxyethane (DME) in LHCEs with a new solvating solvent, 1,2-diethoxyethane (DEE). The new optimal DEE-LHCE exhibits less reactivity against Li_2S_2, alleviates PS dissolution, forms a better cathode−electrolyte interphase layer on the SPAN cathode, and enhances SPAN structural reversibility even at elevated temperatures (45 °C). Compared to DME-LHCE, DEE-LHCE with the same salt and diluent leads to better performance in Li||SPAN batteries (with 82.9% capacity retention after 300 cycles at 45 °C), preservation of the SPAN cathode structure, and suppression of volume change of the Li metal anode. A similar strategy on tailoring the solvating solvents in LHCEs can also be used in other rechargeable batteries to improve their electrochemical performances.

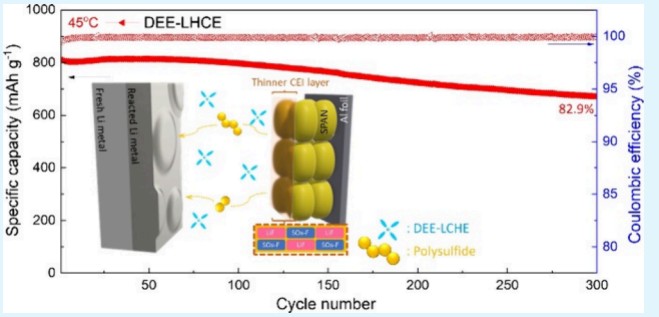

KEYWORDS: *sulfurized polyacrylonitrile, lithium, localized high-concentration electrolyte, solvating solvent, 1,2-diethoxyethane*

INTRODUCTION

The urgent demand for eco-friendly energy sources requires high energy density rechargeable batteries.[1,2] In this regard, lithium (Li)-sulfur (S) batteries have a great potential to be next-generation energy storage systems due to their high theoretical gravimetric energy density (2600 Wh kg^{-1}) and natural abundance of S.[3,4] However, the practical application of Li−S batteries is challenging because of several intrinsic issues. One of which is the continuous generation of polysulfide (PS) species, Li_2S_n ($2 < n \leq 8$) during discharge of elemental S and charge of Li_2S that will transfer from the S cathode side to the Li metal anode inside the battery and react with Li, resulting in loss of active materials, self-discharge through shuttling, and finally poor battery performances.[5,6] As one of the strategies to overcome such issues related to the elemental S cathode, sulfurized polyacrylonitrile (SPAN) is considered an attractive alternative cathode material for S-chemistry batteries since it confines the short chain S species (S_x, $2 \leq x \leq 4$) among PAN chains through chemical bonding to the pyrolyzed pyridine. This structure prevents the formation, dissolution, and shuttling of long chain Li_2S_n species ($4 \leq n \leq 8$) that are always present in elemental S batteries.[7,8] However, the short chain Li_2S_n species ($2 \leq n < 4$) can be formed by breakdown of the C−S and S−S bonds in SPAN during discharging, which can still be dissolved in the electrolytes in Li||SPAN batteries.[9,10] Therefore, alleviating the PS dissolution in SPAN cells is still needed.

For the dissolution of PS during cycling, the electrolyte is a crucial component. The conventional carbonate electrolytes are known for having negligible solubility of PS and thus can limit the crossover of PS. However, it has been reported that the carbonate solvents do not have good compatibility with Li metal anodes.[11] As alternatives, several ether-based electrolytes have been developed for Li||SPAN batteries because many ethers are good solvating solvents and are well-known to be stable with Li metal anodes.[12−15] Among the various solvating solvents, 1,2-dimethoxyethane (DME) was frequently selected due to its excellent stability with Li metal. Lately, our research group introduced a localized high-concentration electrolyte (LHCE) for Li||SPAN batteries. This electrolyte consists of lithium bis(fluorosulfonyl)imide (LiFSI), DME, and 1,1,2,2-

Received: February 8, 2024
Revised: April 3, 2024
Accepted: April 3, 2024
Published: April 15, 2024

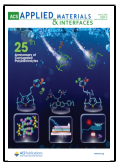

https://doi.org/10.1021/acsami.4c02326
ACS Appl. Mater. Interfaces 2024, 16, 20618−20625

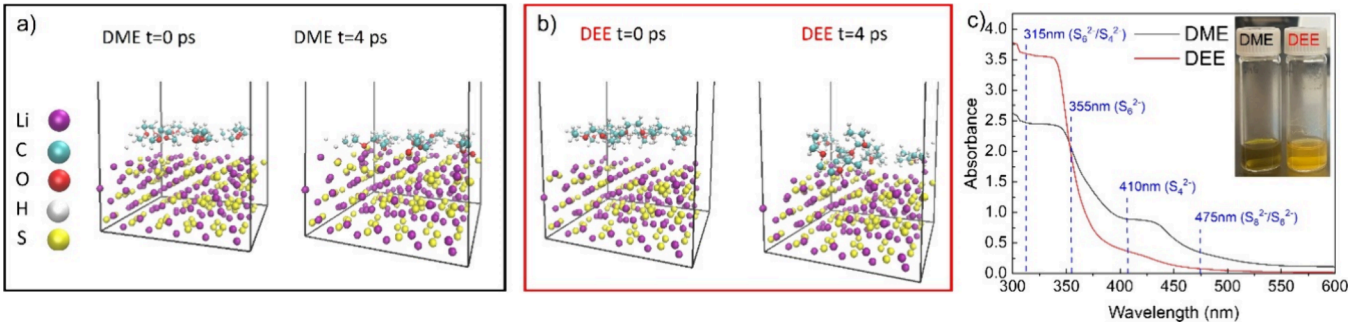

Figure 1. AIMD simulation snapshots of (a) DME and (b) DEE reactivity on Li_2S_2 surface at different periods, respectively. (c) UV−vis spectra after PS solubility test with 0.1 M Li_2S_6 at 55 °C for 20 h in DME and DEE solvents (inset: photo of solvents after PS dissolution).

tetrafluoroethyl-2,2,3,3-tetrafluoropropyl ether (TTE) with a molar ratio of 1:1.2:3.[16] This DME-based LHCE (DME-LHCE) delivered a stable long cyclability over the carbonate-based electrolyte. Furthermore, this DME-LHCE led to outstanding performance of Li||NMC622 batteries due to its good stability with Li metal by forming a salt-derived inorganic-rich solid electrolyte interphase (SEI) layer that is mechanically stable and more ionic conductive on the Li metal anode. However, DME still can lead to PS dissolution, which may become severe at elevated temperatures. In particular, the role of the solvation solvent is crucial in S-based batteries since it is related to both the property of the electrolyte and the S dissolution which affect the battery performance.[17]

To further improve the performance of Li||SPAN batteries, we investigated 1,2-diethoxyethane (DEE) (ethylene glycol diethyl ether), an analogue of DME, as an alternative solvating solvent in LHCEs. Since DEE has a longer alkyl chain than DME, it is expected to have less reactivity with Li_2S_2 and improve cycling performance of Li||SPAN batteries, particularly at elevated temperatures. Moreover, benefiting from the intrinsic chemical structure of LHCEs, DEE-based LHCE (DEE-LHCE) may form both a stable SEI layer on the Li metal anode and a robust cathode−electrolyte interphase (CEI) layer on the SPAN cathode during cycling. In this study, the compatibilities of DEE-LHCE and DME-LHCE electrolytes with both the SPAN cathode and Li metal anode were systematically investigated. The interphase phenomena and cycling performance of Li||SPAN batteries using optimized DEE-LHCE and DME-LHCE are compared. This study demonstrates how to design the solvating solvent of LHCEs for Li||SPAN batteries and enables high energy density Li-based batteries.

RESULTS AND DISCUSSION

DME versus DEE: Compatibility between Solvating Solvent and SPAN Cathode. As mentioned above, Li_2S_x ($2 \leq x \leq 4$) dissolution and crossover to the Li metal anode need to be alleviated to get improved cyclability of Li||SPAN batteries. To compare the reactivity of DME and DEE with that of Li_2S_x, Li_2S_2 was selected as a representative for conducting Ab initio molecular dynamics (AIMD) simulations. In the beginning, both DME and DEE are a bit away from the Li_2S_2 surface. When t = 4 ps, most DME molecules move close to the Li_2S_2 surface and the binding between Li in Li_2S_2 and oxygen (O) in DME molecules is detected (Figure 1a). While DEE molecules partially move toward the Li_2S_2 surface at t = 4 ps, suggesting that Li_2S_2 prefers to adsorb DME over DEE (Figure 1b). Since DEE has longer alkyl chain than DME, DEE is supposed to be less lithophilic than DME. The density function theory (DFT)-based reactivity descriptors such as local softness and local hardness have been used as reactivity indices to predict the reactivity sequences of chemical compounds.[18−20] As the reactions between PSs (here mostly Li_2S_2) and ether solvents in Li−S batteries are usually considered as nucleophilic attack,[21] we calculated the condensed local softness (LS^+) descriptor of the solvents, i.e., DME and DEE in the electrolytes, to evaluate their reactivities with Li_2S_2. Since the target is the C−O bond of ether in the reaction, either the descriptor of the C or the O atom could be the indicator. Here we used the LS^+ of O atom because we found that the correlation between the LS^+ of O atom in ether and the reaction activation enthalpy[21] of Li_2S_2-ether is better than that of C atom. Normally, a higher LS^+ value indicates a higher reactivity. The calculated LS^+ values for the O atom in DME and DEE are 0.0741 and 0.0539 eV^{-1}, respectively, suggesting that the reactivity of DEE is lower than that of DME in the reaction between PS and solvent.

To elucidate the PS solubility in the solvating solvents, 0.1 M Li_2S_6 solutions were prepared with DME and DEE, respectively, by stirring at 55 °C for 20 h. The DME solution shows a dark brown color, while the DEE solution is just light yellow as shown in a photo in the inset of Figure 1c. To further quantify the solubility, UV−Vis spectra of the solutions are obtained (Figure 1c). DEE solution presents a higher absorbance peak of 315 nm corresponding to S_6^{2-}/S_4^{2-} than DME solution, but its other peaks at 355, 410, and 475 nm (corresponding to S_6^{2-}, S_4^{2-}, and S_8^{2-}/S_6^{2-}, respectively)[15,22] are less detected than in DME solution. These results demonstrate that DEE reduces the PS solubility compared to DME.

Even though the DME-LHCE (LiFSI:DME:TTE = 1:1.2:3 by mol.) was reported as a good electrolyte to enable an improved cycle life of Li||SPAN battery over the conventional carbonate-based electrolyte,[11,16] it is considered that DEE in LHCE could bring further improvement based on the above findings. To optimize the DEE-LHCE formulation, the electrochemical properties of LHCEs with the LiFSI salt, DEE solvating solvent, and TTE diluent at various molar ratios were tested. Figure S1a exhibits the curves of Li deposition and stripping in Li||copper (Cu) cells to measure the average Li Coulombic efficiency (CE) of these LHCEs along with the HCE of LiFSI-DEE at 1:1 by mol. It is seen that the LHCEs of LiFSI-DEE-TTE with various molar ratios have very little difference in Li CE. However, the six DEE-based LHCEs in Li||SPAN cells show different cycling performance at a current density of C/5 (where 1C = 3 mA cm^{-2}) in a voltage range

https://doi.org/10.1021/acsami.4c02326
ACS Appl. Mater. Interfaces 2024, 16, 20618−20625

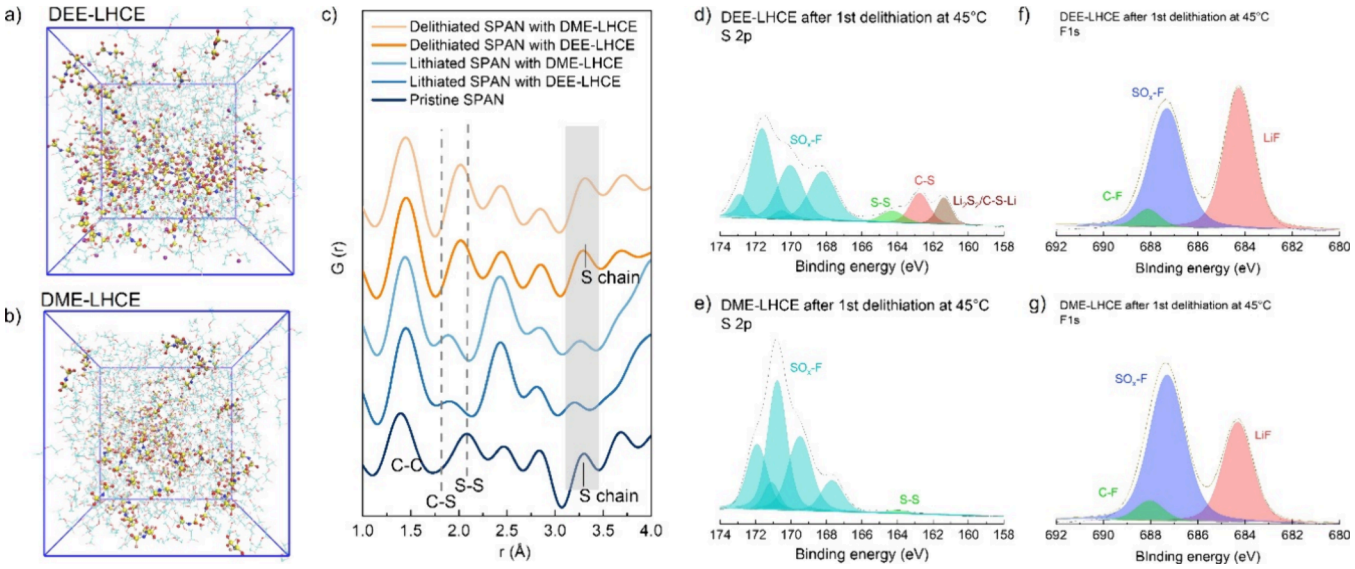

Figure 2. Snapshots of the final state (a) DEE-LHCE and (b) DME-LHCE at ET (45 °C) obtained by the CMD simulations. The LiFSI clusters are highlighted. (c) PDF results of SPAN cathodes using DEE-LHCE and DME-LHCE. XPS S 2p spectra of SPAN electrodes after first delithiation at 45 °C using (d) DEE-LHCE and (e) DME-LHCE. XPS F 1s spectra of SPAN electrodes after first delithiation at 45 °C using (f) DEE-LHCE and (g) DME-LHCE.

from 1.0 to 3.0 V at 25 °C (Figure S1b). The cell with LHCE of LiFSI:DEE:TTE (1:1:2 by mol.) delivers 82% capacity retention after 500 cycles, while others do not reach there stably, so the composition of LiFSI:DEE:TTE (1:1:2 by mol.) is selected as the optimal DEE-LHCE for further studies.

Solvating Solvent Effect on Li|SPAN Performance. To investigate the effect of solvating solvents on the performance of Li|SPAN batteries, DME-LHCE (i.e., LiFSI-1.2DME-3TTE by mol.) and the optimal DEE-LHCE (i.e., LiFSI-1DEE-2TTE by mol.) are compared under the electrochemical tests. Both show very similar average Li CE of around 99.4∼99.5% in Li|Cu cells, but DEE-LHCE has slightly higher polarization than DME-LHCE (Figure S2a). The latter is possibly related to the fact that DEE-LHCE has a lower ionic conductivity (Figure S2b). When checking the morphology of the deposited Li in the two LHCEs for an areal capacity of 2 mAh cm^{-2} at a current density of 1 mA cm^{-2}, it is found that both LHCEs lead to similar size of granular Li particles, but DEE-LHCE yields a slightly denser Li deposition morphology (Figure S3). Furthermore, as exhibited in Figure S2c about Sand's capacity with current density for the two electrolytes, DEE-LHCE has a higher Sand's capacity, implying that DEE-LHCE could prevent dendrite growth better than DME-LHCE.[23] These results indicate that DME-LHCE and DEE-LHCE have good compatibility with the Li metal anode and DEE-LHCE would behave better in Li|SPAN cells. This can be verified by the cycling stability of the Li|SPAN cells with the two LHCEs. As shown in Figure S4, the cells with DME-LHCE exhibited a sudden capacity drop after 300 cycles, while the cells with DEE-LHCE demonstrated a stable cycle life with capacity retention of 80% after 500 cycles when the Li|SPAN cells were cycled at a current density of C/10 (where 1C = 3 mA cm^{-2}) at 25 °C. Of course, the better cycle life of the Li|SPAN cells with DEE-LHCE than that with DME-LHCE could also relate to the higher compatibility of DEE-LHCE with the SPAN cathode than DME-LHCE does, as the aforementioned difference in local softness values for the two solvating solvents DEE and DME.

In the LHCEs, contact ion pairs (CIPs, anion coordinating to a single Li ion) and aggregated clusters (AGGs, anion coordinating to two or more Li ions) allow rapid migration of the FSI anion from the electrolyte to the surface of the Li metal anode and reductive decomposition.[24] Although the coordination number (CN) between Li ion and solvating solvent, anion, and diluent in both DME-LHCE and DEE-LHCE is not much changed at varied temperatures (Figure S5), the slightly higher CN between Li^+ and FSI^- in DEE-LHCE (2.3) than in DME-LHCE (2.0) suggests there is a higher total number of CIPs and AGGs in DEE-LHCE; thus, there is higher possibility of forming more anion-derived SEI on Li and CEI on SPAN. The proportion of CIPs and AGGs is further extracted from MD simulations. DEE-LHCE presents a higher AGG ratio of 74.2% than DME-LHCE (60.9%) at 25 °C. Even though the AGG ratio of both LHCEs is slightly reduced at 45 °C, DEE-LHCE preserves a relatively higher AGG ratio (71.8%) compared to DME-LHCE has (59.3%). The CIP ratios in DEE-LHCE (1.8% at 25 °C and 2.3% at 45 °C) are slightly less than those in DME-LHCE (5.3% at 25 °C and 4.2% at 45 °C). However, the total ratio of AGG and CIP in DEE-LHCE is still higher than that in DME-LHCE, 76.0 vs 65.2% at 25 °C and 74.1 vs 63.5% at 45 °C. Higher content of AGGs and CIPs would result in more salt-derived SEI on Li metal anodes and CEI on SPAN cathodes in DEE-LHCE, which corroborates well with the XPS results and the battery performance. Besides, DEE-LHCE tends to have a larger cluster size than DME-LHCE, especially at elevated temperature (45 °C) rather than room temperature (25 °C) as shown in Figures 2a,b, and S6. Benefiting from this, DEE-LHCE could have a better CEI on the SPAN cathode and bring good electrochemical performance of Li|SPAN cells.

To delve into the interphase phenomena, the SPAN structure and the CEI layer are closely investigated with the SPAN cathode after one cycle at 45 °C via X-ray pair distribution function (PDF) characterization and X-ray photoelectron spectroscopy (XPS). It is known that S−S bonds will break at the lithiation and rebond after delithiation

https://doi.org/10.1021/acsami.4c02326
ACS Appl. Mater. Interfaces 2024, 16, 20618−20625

Scheme 1. Schematic Illustration of Advantages of DEE-LHCE Compared to DME-LHCE in Li||SPAN Batteries

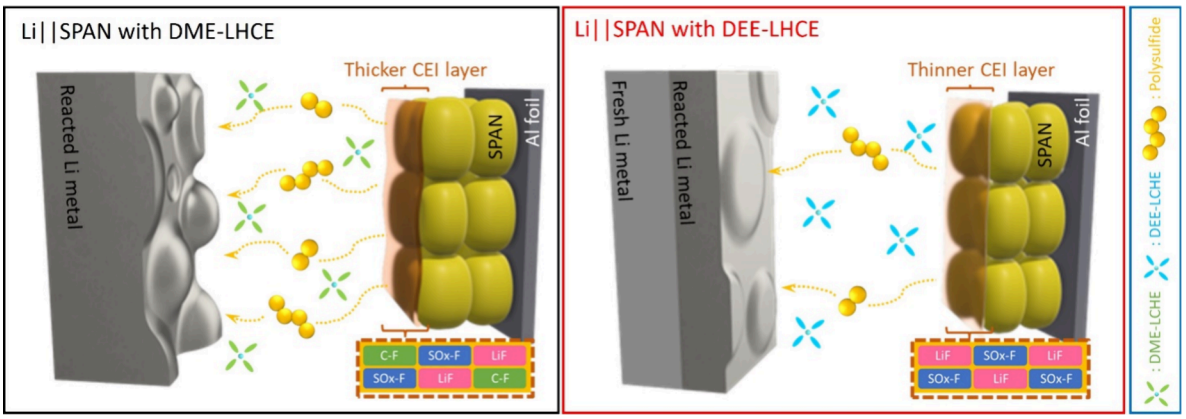

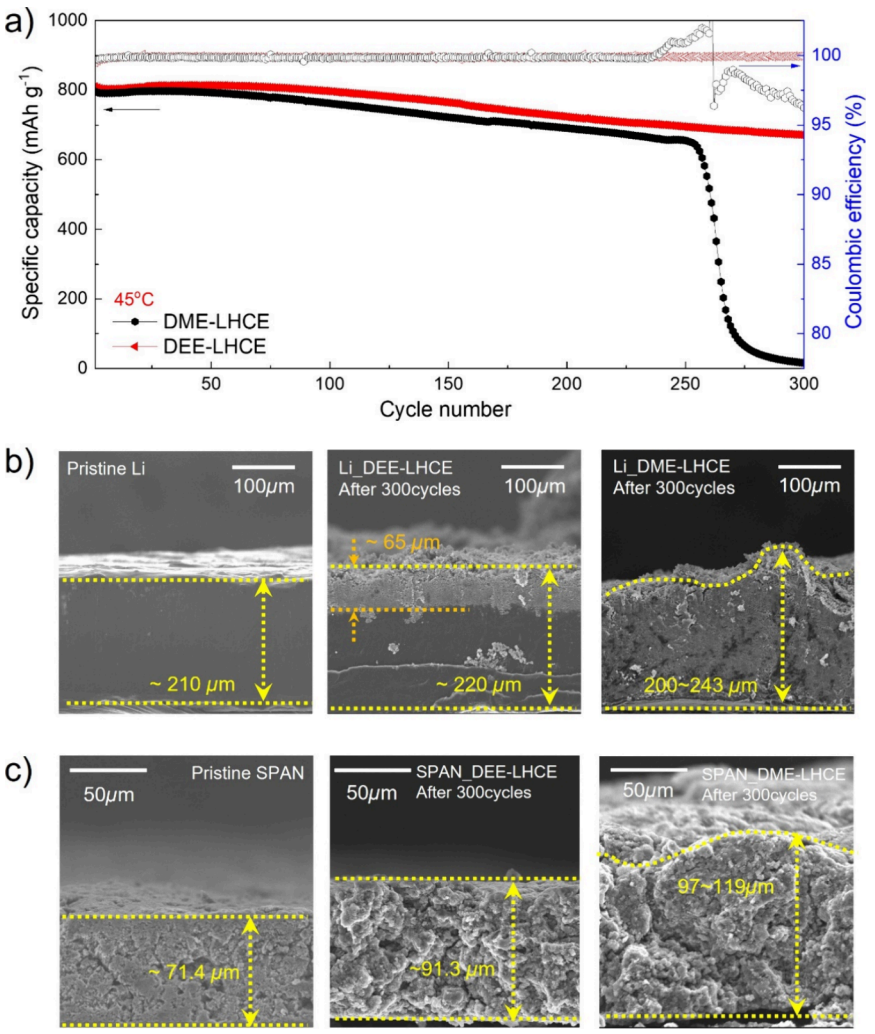

Figure 3. (a) Cycle performance of Li||SPAN cells at a current density of C/5 using DME-LHCE and DEE-LHCE at 45 °C. (b, c) Cross-sectional SEM images of (b) Li metal anodes and (c) SPAN electrodes from Li||SPAN cells before and after 300 cycles.

and C−S bonds will be generated by C−S−Li interaction during lithiation and delithiation.[25] The PDF results shown in Figure 2c indicate that the lithiated SPAN cathode with DEE-LHCE presents the C−S bond of around 1.9 Å long and its length decreases after delithiation, indicating the recovery of the SPAN cathode structure. Further, the S−S bond (at around 3.3 Å length) gets stronger after delithiation according to the formation of S chain.[25] DME-LHCE exhibits a similar behavior, confirming that SPAN cathode structure recovered as well. Figure 2d presents the S−S bond (~164.0 eV) in S 2p spectra of the SPAN cathode cycled with DEE-LHCE, indicating the reversibility of S−S and C−S bonds (~162.2 eV, S 2p)[26,27] like the pristine SPAN exhibits (Figure S7) after the breakage of Li−S bonds. However, the complete recovery

https://doi.org/10.1021/acsami.4c02326
ACS Appl. Mater. Interfaces 2024, 16, 20618−20625

of the SPAN structure after cycling is difficult since some of Li is still bonded to S as Li_2S_2/C−S−Li (~161.6 eV, S 2p).[16] On the SPAN cathode cycled with DME-LHCE, not only Li_2S_2/C−S−Li and C−S are not detected but S−S bonds are weaker than the SPAN cycled with DEE-LHCE, while its SO_x−F is observed at higher intensity (Figure 2d vs. e).

Intriguingly, a strong SO_x−F peak (686.5 eV, F 1s) is detected on both SPAN cathodes with DEE-LHCE and DME-LHCE, but LiF (684.7 eV, F 1s) is more significant on the SPAN cycled with DEE-LHCE with the concentration of 47.5%, while DME-LHCE shows 31.4% of the concentration (Figure 2e,f).[28,29] On the Li anodes, DEE-LHCE forms the SEI layer including LiF as shown in Figure S8b, while LiF is not indicated on the formed SEI layer by DME-LHCE (Figure S8c). LiF is a well-known species that can help improve ion transport through the CEI and SEI layers at certain amount.[30,31] In addition, DEE-LHCE brings less resistance (~12.2 Ω) after the first cycle at 45 °C compared to DME-LHCE (~21.7 Ω) even though both have a very similar capacity during formation and impedance after the formation at 25 °C (Figure S9a,b). Also, DEE-LCHE brought a higher specific capacity (813.5 mAh g^{-1}) than DME-LHCE (793.6 mAh g^{-1}, Figure S9b). Based on these results, it can be concluded that DEE-LHCE could form a better CEI layer on the SPAN cathode and a more robust SEI on the Li anode, which promotes a better cycling performance of the battery at 45 °C than DME-LHCE does. The advantages of DEE-LHCE in Li||SPAN battery are depicted in Scheme 1.

Cycling Performance of Li||SPAN Batteries and Postmortem Analysis. The cycling performance of Li|| SPAN batteries in DME-LHCE and DEE-LHCE at 45 °C was conducted at a current density of C/5 (where 1C = 3 mA cm^{-2}) under the voltage range from 1.0 to 3.0 V. Benefiting from a less reactivity with PS and a better interphase on SPAN cathodes of DEE-LHCE, a higher initial capacity and an enhanced capacity retention (82.9% after 300 cycles) were obtained compared to DME-LHCE (~0% after 300 cycles) that showed drastic capacity decay after 250 cycles as shown in Figure 3a. Even though DME-LHCE has a higher ionic conductivity (5.03 mS cm^{-1} at 45 °C) than DEE-LHCE (3.06 mS cm^{-1} at 45 °C, Figure S2b), the cycle life of Li||SPAN cells using DEE-LHCE is improved based on the alleviated reactivity against PS and the well-established interphase layers. This result underlines that the interphase reaction rather than the bulk property of the electrolyte plays a dominant role in the electrochemical performance of the Li||SPAN batteries.

After 300 cycles, the cycled Li and SPAN electrodes were further characterized. Figure S10 shows that the Li metal anode cycled with DEE-LHCE has a relatively denser and smoother surface than Li with DME-LHCE. Furthermore, the cross-sectional scanning electron microscopy (SEM) images present that Li cycled with DEE-LHCE preserves a thicker unreacted Li metal layer by suppressing the generation of reacted or corroded Li layer possibly with "dead" Li on the Li metal anode during cycling (Figure 3b). In contrast, the Li metal anode from Li||SPAN cells with DME-LHCE shows a complete change to reacted or corroded Li with byproducts through the thickness direction and accompanying a larger volume change indicating more side reactions occurred during cycling. It is demonstrated that the SEI layer having more salt-derived species helps enhance the long stability of Li metal anodes. With a better CEI layer on the SPAN cathode from DEE-LHCE, the SPAN cathode maintains the structure well after 300 cycles, while the SPAN cathode with DME-LHCE shows more aggregation and collapse (Figure S11). Although S species are chemically bonded on the PAN chains in SPAN, there is still concern about the volume changes on SPAN cathodes by repeated lithiation and delithiation.[32] Besides, it is assumed that the volume expansion of SPAN cathode could be severe at elevated temperatures owing to the further side reactions and byproducts formation. It is observed that SPAN cathodes can be swollen even after soaking in both electrolytes, with the thickness increase by 21.4% in DEE-LHCE and 23.2% in DME-LHCE (Figure S12a,b) compared to the pristine SPAN cathode (~71.4 μm, Figure 3c). After the formation cycle, the SPAN cathodes show the volume expansion at the thickness increase of 27.7% with DEE-LHCE and 35.6% with DME-LHCE, respectively (Figure S12c,d) compared to the pristine SPAN cathode. After 300 cycles, the SPAN cathode from the Li||SPAN cell with DEE-LHCE shows a thickness of ~91.3 μm, a 27.9% increase compared with the pristine SPAN cathode (Figure 3c). However, the SPAN cathode cycled in DME-LHCE exhibits a thickness of 97~119 μm, an increase of 35.9~66.6% over the pristine SPAN electrode. These results indicate that a well-tailored solvating solvent for LHCEs has a crucial role in the performance of Li||SPAN batteries not only due to its compatibility on both Li and SPAN electrodes, but also due to its reduced interphasial side reactions on both electrodes, leading to enhanced Li||SPAN battery cycle life even at elevated temperatures.

CONCLUSIONS

This study reveals the crucial role of a solvating solvent in LHCEs for Li||SPAN batteries. DME has been applied as a solvating solvent in LHCEs due to its good compatibility with Li metal anode; however, it has certain reactivity against PS, which causes limited cycle life of Li||SPAN batteries. Here, DEE is suggested and investigated since compared to DME it has less reactivity with PS and more coordination with FSI^- which could form better interphase layers (SEI and CEI) with more salt-derived species on both electrodes. DEE-based LHCEs are designed with the same salt and diluent as DME-LHCE of LiFSI-1.2DME-3TTE (by mol.) to elucidate the effect of the solvating solvent. Benefiting from the virtues of DEE over DME, the optimal DEE-LHCE, LiFSI-1DEE-2TTE by mol., has better compatibility with Li metal anode and SPAN cathode, thus enabling Li||SPAN batteries to deliver a longer cycle life at both room temperature and elevated temperature. Especially, improved interphase in Li||SPAN using DEE-LHCE effectively alleviates the generation of byproducts and volume changes on both Li metal anode and SPAN cathode even at elevated temperature. This study demonstrates the crucial role of the solvating solvent in LHCEs to the Li||SPAN batteries and helps tailor the electrolytes to achieve the long lifespan of high energy density batteries.

EXPERIMENTAL METHODS

Preparation of Electrolytes. Lithium bis(fluorosulfonyl)imide (LiFSI, battery grade) was obtained from Nippon Shokubai and further dried at ~100 °C under vacuum overnight prior to use. 1,2-Dimethoxyethane (DME, battery grade) was purchased from Gotion and used as received. 1,2-Diethoxyethane (DEE, 99%, from Oakwood Chemical) and 1,1,2,2-tetrafluorethyl-2,2,3,3-tetrafluoropropyl ether (TTE, 97%, from SynQuest Laboratories) were acquired and dried with preactivated molecular sieves until the moisture content was less

https://doi.org/10.1021/acsami.4c02326
ACS Appl. Mater. Interfaces 2024, 16, 20618−20625

than 20 ppm by Karl Fisher titration. The studied localized high concentration electrolytes (LHCEs) were prepared stepwise following the ratio presented in the manuscript (DME-LHCE: LiFSI-DME-TTE at 1:1.2:3 by mol.), DEE-LHCEs: LiFSI-DEE-TTE at 1:a:b by mol., where $0.9 \leq a \leq 1.2$, $1 \leq b \leq 3$). LiFSI salt was first dissolved in each solvating solvent (DME or DEE) until completion, and then TTE was added to the solution as a diluent. All the process was conducted inside a glovebox (MBraun) filled with purified argon (Ar), where both oxygen and moisture were kept below 0.1 ppm.

Electrochemical Tests. CR2032 coin cell kits were used for electrochemical performance tests. The sulfurized polyacrylonitrile (SPAN) cathode was composed of SPAN powder, carbon black (SuperP), and carboxymethyl cellulose (CMC) binder at 8:1:1 by weight ratio on the carbon-coated aluminum (Al) current collector. The cathode areal capacity loading was around 3 mAh cm^{-2}. The 20 μm polyethylene (PE) separator (Energy Tech Solution), 30 μL of the electrolyte, and 210 μm thick Li metal chip as the anode were used. The Li||SPAN cells were cycled on Landt battery testers at C/5 (where 1C = 3 mA cm^{-2}) at 25 and 45 °C, after two formation cycles of charge/discharge cycle at C/10 at 25 °C in the voltage range from 1.0 to 3.0 V. The cycling performance was conducted with three parallel coin cells for each electrolyte. The average Li Coulombic efficiency (CE) of the electrolytes was measured in Li||Cu (copper) cells by the following procedures: A capacity of 5 mAh cm^{-2} Li metal was electrochemically deposited onto the bare Cu electrode at a current density of 0.5 mA cm^{-2} and then fully stripped until a cutoff voltage of 1 V (vs Li/Li^+). Another 5 mAh cm^{-2} of Li metal was deposited, and 1.0 mAh cm^{-2} of Li metal was repeatedly stripped and deposited at a current density of 0.5 mA cm^{-2} for ten cycles. In the final step, all of the remaining Li metal was stripped at a current density of 0.5 mA cm^{-2}. The ionic conductivities of the LHCEs were measured on a Bio-Logic MCS from −20 to 60 °C. The interphase resistance was examined by an AC impedance analysis (VSP classic, Bio-Logic) over a frequency range of 10^{-2}–10^{6} Hz at room temperature. The Sand's capacities of the electrolytes were calculated following Sand's formula.[23]

Structural/Physicochemical Characterizations. To check the color changes of the solvating solvents and to measure UV−vis, the polysulfide (PS) solubility test was performed with 0.1 M Li_2S_6 at 55 °C for 20 h. The supernatants from the solvating solvents were transferred into Globe Scientific Spectrophotometer Cuvettes (Fisher Scientific) and analyzed by using a UV−vis spectrophotometer (UV−vis 2501PC, Shimadzu) at a scan rate of 0.5 nm s^{-1}, covering a wavelength range from 800 to 200 nm. X-ray photoelectron spectroscopy (XPS) analysis was conducted on a Physical Electronics Quantera Scanning X-ray Microprobe (Physical Electronics, Germany), which uses a focused monochromatic Al Kα (1486.7 eV) source for excitation. High-energy resolution S 2p and F 1s spectra were collected using a pass-energy of 69 eV with a step size of 0.125 eV. The obtained spectra were fitted with the CasaXPS software with the binding energy was calibrated with C 1s at 284.8 eV. Pair distribution function (PDF) characterization was carried out on the cycled SPAN samples in the beamline 28-ID-2 at National Synchrotron Radiation Lightsource II (NSLS II) at Brookhaven National Laboratory. The cycled SPAN powder was scrapped off from the current collector. Polyimide tube of 4 cm in length and 0.05" internal diameter was used to collect the samples. One cm at one end and 2 cm at the other end of the tube were sealed with epoxy glue inside an Ar-filled glovebox to prevent air exposure of the samples. Samples were then exposed to an X-ray beam of 0.1814 Å with 2 min exposure time. Each sample was scanned 5 times. The data integration was performed in Dioptas,[33] and PDF data were extracted using PDFgetX3.[34] The surface and cross-sectional images were observed by Helios scanning electron microscopy (SEM). For the postmortem analyses, the electrodes were collected after the coin cell disassembly and gently washed with DME or DEE solvent to remove the electrolyte residues.

Simulations. Density functional theory (DFT) calculations were performed using the B3LYP functional with ORCA package.[35] The geometries of the molecules were optimized with the 6-31G** basis. Vibrational frequencies were calculated for validation of the stable configuration. An effect of implicit solvent model with acetone was included via COSMO model.[36] The condensed local softness descriptors of DME and DEE were calculated by Multiwfn software.[37]

■ ASSOCIATED CONTENT

Supporting Information

The Supporting Information is available free of charge at https://pubs.acs.org/doi/10.1021/acsami.4c02326.

Electrochemical measurements including average Coulombic efficiency, ionic conductivity, Sand's capacity, and cycle performance of Li||SPAN batteries of LHCEs; XPS spectra; AIMD simulation results; and SEM images of both Li metal anodes and SPAN cathodes after cycling (PDF)

■ AUTHOR INFORMATION

Corresponding Authors

Ji-Guang Zhang − *Energy and Environment Directorate, Pacific Northwest National Laboratory, Richland, Washington 99354, United States;* orcid.org/0000-0001-7343-4609; Email: jiguang.zhang@pnnl.gov

Wu Xu − *Energy and Environment Directorate, Pacific Northwest National Laboratory, Richland, Washington 99354, United States;* orcid.org/0000-0002-2685-8684; Email: wu.xu@pnnl.gov

Authors

Ju-Myung Kim − *Energy and Environment Directorate, Pacific Northwest National Laboratory, Richland, Washington 99354, United States;* orcid.org/0000-0003-0851-1959

Peiyuan Gao − *Physical and Computational Sciences Directorate, Pacific Northwest National Laboratory, Richland, Washington 99354, United States;* orcid.org/0000-0002-2906-6551

Qiushi Miao − *Department of NanoEngineering, University of California San Diego, La Jolla, California 92093, United States;* orcid.org/0009-0008-0857-6107

Qian Zhao − *Earth and Biological Sciences Directorate, Pacific Northwest National Laboratory, Richland, Washington 99354, United States;* orcid.org/0000-0003-4489-3691

Muhammad Mominur Rahman − *Chemistry Division, Brookhaven National Laboratory, Upton, New York 11973, United States*

Ping Chen − *Physical and Computational Sciences Directorate, Pacific Northwest National Laboratory, Richland, Washington 99354, United States*

Xin Zhang − *Physical and Computational Sciences Directorate, Pacific Northwest National Laboratory, Richland, Washington 99354, United States;* orcid.org/0000-0003-2000-858X

Enyuan Hu − *Chemistry Division, Brookhaven National Laboratory, Upton, New York 11973, United States;* orcid.org/0000-0002-1881-4534

Ping Liu − *Department of NanoEngineering, University of California San Diego, La Jolla, California 92093, United States;* orcid.org/0000-0002-1488-1668

Complete contact information is available at: https://pubs.acs.org/10.1021/acsami.4c02326

Author Contributions

W.X. and J.-M.K. designed the experiments with inputs from J.-G.Z. J.-M.K. conducted the electrochemical performance. P.G.

https://doi.org/10.1021/acsami.4c02326
ACS Appl. Mater. Interfaces 2024, 16, 20618−20625

conducted simulations. Q.M. and P.L. prepared SPAN cathodes. Q.Z. obtained XPS spectra. M.M.R. and E.H. conducted PDF. P.C. and X.Z. performed UV−vis measurement. J.-M.K., J.-G.Z., and W.X. contributed to the manuscript preparation. All the authors discussed the experimental results and commented on the manuscript.

Notes

The authors declare no competing financial interest.

■ ACKNOWLEDGMENTS

This work was supported by the Assistant Secretary for Energy Efficiency and Renewable Energy, Vehicle Technologies Office, of the U.S. Department of Energy (DOE) through the Advanced Battery Materials Research program (Battery500 Consortium) under the contract no. DE-AC05-76RL01830. The XPS characterization was supported under a partial grant from the Washington State Department of Commerce's Clean Energy Fund and performed at the Environmental Molecular Sciences Laboratory, a DOE Office of Science User Facility sponsored by the Office of Biological and Environmental Research and located at Pacific Northwest National Laboratory (PNNL). PNNL is operated by Battelle for the DOE under Contract DE-AC05-76RL01830. The LiFSI salt was provided by Dr. Kazuhiko Murata of Nippon Shokubai Co., Ltd.

■ REFERENCES

(1) Wen, J.; Zhao, D.; Zhang, C. An overview of electricity powered vehicles: Lithium-ion battery energy storage density and energy conversion efficiency. *Renew. Energy* **2020**, *162*, 1629−1648.

(2) Abbas, Q.; Mirzaeian, M.; Hunt, M. R.; Hall, P.; Raza, R. Current state and future prospects for electrochemical energy storage and conversion systems. *Energies* **2020**, *13* (21), 5847.

(3) Chen, S.; Yu, Z.; Gordin, M. L.; Yi, R.; Song, J.; Wang, D. A Fluorinated Ether Electrolyte Enabled High Performance Prelithiated Graphite/Sulfur Batteries. *ACS Appl. Mater. Interfaces* **2017**, *9* (8), 6959−6966.

(4) Zhou, G.; Chen, H.; Cui, Y. Formulating energy density for designing practical lithium−sulfur batteries. *Nat. Energy* **2022**, *7* (4), 312−319.

(5) Shi, Z.; Li, M.; Sun, J.; Chen, Z. Defect engineering for expediting Li−S chemistry: strategies, mechanisms, and perspectives. *Adv. Energy Mater.* **2021**, *11* (23), No. 2100332.

(6) Li, G.; Huang, Q.; He, X.; Gao, Y.; Wang, D.; Kim, S. H.; Wang, D. Self-Formed Hybrid Interphase Layer on Lithium Metal for High-Performance Lithium−Sulfur Batteries. *ACS Nano* **2018**, *12* (2), 1500−1507.

(7) Kumar, R.; Liu, J.; Hwang, J.-Y.; Sun, Y.-K. Recent research trends in Li−S batteries. *J. Mater. Chem. A* **2018**, *6* (25), 11582−11605.

(8) Chen, W. J.; Li, B. Q.; Zhao, C. X.; Zhao, M.; Yuan, T. Q.; Sun, R. C.; Huang, J. Q.; Zhang, Q. Electrolyte regulation towards stable lithium-metal anodes in lithium−sulfur batteries with sulfurized polyacrylonitrile cathodes. *Angew. Chem. Inter. Ed.* **2020**, *59* (27), 10732−10745.

(9) Zhao, X.; Wang, C.; Li, Z.; Hu, X.; Razzaq, A. A.; Deng, Z. Sulfurized polyacrylonitrile for high-performance lithium sulfur batteries: advances and prospects. *J. Mater. Chem. A* **2021**, *9* (35), 19282−19297.

(10) Shen, Z.; Zhang, W.; Mao, S.; Li, S.; Wang, X.; Lu, Y. Tailored electrolytes enabling practical lithium−sulfur full batteries via interfacial protection. *ACS Energy Lett.* **2021**, *6* (8), 2673−2681.

(11) Miao, Q.; Solan, N.; Hyun, G.; Holoubek, J.; Liu, P. Electrolyte Engineering for Long-Life Li-SPAN Batteries. *ACS Energy Lett.* **2023**, *8* (11), 4818−4830.

(12) Wu, Z.; Liu, H.; Holoubek, J.; Anderson, C.; Shi, L.; Khemchandani, H.; Lu, D.; Liu, D.; Niu, C.; Xiao, J. The Role of Ion Transport in the Failure of High Areal Capacity Li Metal Batteries. *ACS Energy Lett.* **2022**, *7* (8), 2701−2710.

(13) Ma, T.; Ni, Y.; Li, D.; Zha, Z.; Jin, S.; Zhang, W.; Jia, L.; Sun, Q.; Xie, W.; Tao, Z. Reversible Solid−Solid Conversion of Sulfurized Polyacrylonitrile Cathodes in Lithium−Sulfur Batteries by Weakly Solvating Ether Electrolytes. *Angew. Chem. Int. Ed.* **2023**, *62* (43), No. e202310761.

(14) Liu, H.; Holoubek, J.; Zhou, H.; Chen, A.; Chang, N.; Wu, Z.; Yu, S.; Yan, Q.; Xing, X.; Li, Y. Ultrahigh coulombic efficiency electrolyte enables Lill SPAN batteries with superior cycling performance. *Mater. Today* **2021**, *42*, 17−28.

(15) Xing, X.; Li, Y.; Wang, X.; Petrova, V.; Liu, H.; Liu, P. Cathode electrolyte interface enabling stable Li−S batteries. *Energy Storage Mater.* **2019**, *21*, 474−480.

(16) Zhang, X.; Gao, P.; Wu, Z.; Engelhard, M. H.; Cao, X.; Jia, H.; Xu, Y.; Liu, H.; Wang, C.; Liu, J.; Zhang, J.-G.; Liu, P.; Xu, W. Pinned Electrode/Electrolyte Interphase and Its Formation Origin for Sulfurized Polyacrylonitrile Cathode in Stable Lithium Batteries. *ACS Appl. Mater. Interfaces* **2022**, *14* (46), 52046−52057.

(17) Su, C.-C.; He, M.; Amine, R.; Chen, Z.; Amine, K. The Relationship between the RelativeSolvatingPowerofElectrolytesand ShuttlingEffectof LithiumPolysulfidesin Lithium−SulfurBatteries. *Angew. Chem., Int. Ed.* **2018**, *57*, 12033−12036.

(18) Roy, R. K.; Krishnamurti, S.; Geerlings, P.; Pal, S. Local Softness and Hardness Based Reactivity Descriptors for Predicting Intra- and Intermolecular Reactivity Sequences: Carbonyl Compounds. *J. Phys. Chem. A* **1998**, *102* (21), 3746−3755.

(19) Domingo, L. R.; Chamorro, E.; Pérez, P. Understanding the Reactivity of Captodative Ethylenes in Polar Cycloaddition Reactions. *A Theoretical Study. J. Org. Chem.* **2008**, *73* (12), 4615−4624.

(20) Chattaraj, P. K.; Sarkar, U.; Roy, D. R. Electrophilicity Index. *Chem. Rev.* **2006**, *106* (6), 2065−2091.

(21) Assary, R. S.; Curtiss, L. A. Molecular Level Understanding of the Interactions Between Reaction Intermediates of Li−S Energy Storage Systems and Ether Solvents. In *Lithium−Sulfur Batteries*; Wiley, 2019; pp. 133−146.

(22) Häcker, J.; Nguyen, D. H.; Rommel, T.; Zhao-Karger, Z.; Wagner, N.; Friedrich, K. A. Operando UV/vis spectroscopy providing insights into the sulfur and polysulfide dissolution in magnesium−sulfur batteries. *ACS Energy Lett.* **2022**, *7* (1), 1−9.

(23) Bai, P.; Li, J.; Brushett, F. R.; Bazant, M. Z. Transition of lithium growth mechanisms in liquid electrolytes. *Energy Environ. Sci.* **2016**, *9* (10), 3221−3229.

(24) Cao, X.; Jia, H.; Xu, W.; Zhang, J.-G. Localized high-concentration electrolytes for lithium batteries. *J. Electrochem. Soc.* **2021**, *168* (1), No. 010522.

(25) Tan, S.; Rahman, M. M.; Wu, Z.; Liu, H.; Wang, S.; Ghose, S.; Zhong, H.; Waluyo, I.; Hunt, A.; Liu, P. Structural and Interphasial Stabilities of Sulfurized Polyacrylonitrile (SPAN) Cathode. *ACS Energy Lett.* **2023**, *8*, 2496−2504.

(26) Murugan, S.; Niesen, S.; Kappler, J.; Küster, K.; Starke, U.; Buchmeiser, M. R. Ultra-Stable Cycling of High Capacity Room Temperature Sodium-Sulfur Batteries Based on Sulfurated Poly (acrylonitrile). *Batteries Supercaps* **2021**, *4* (10), 1636−1646.

(27) Wang, Y.; Li, M.; Wen, T.; Gu, G. A 3D COF constructed by interlayer crosslinking of 2D COF as cathode material for lithium-sulfur batteries. *Nanotechnology* **2023**, *34*, 375402 DOI: 10.1088/1361-6528/acddef.

(28) Chang, X.; Liu, H.; Yang, H.; Di, J.; Tang, W.; Fu, H.; Li, M.; Liu, R. Co-guiding the dendrite-free plating of lithium on lithiophilic ZnO and fluoride modified 3D porous copper for stable Li metal anode. *J. Mater.* **2020**, *6* (1), 54−61.

(29) Li, Y.; Liu, M.; Wang, K.; Li, C.; Lu, Y.; Choudhary, A.; Ottley, T.; Bedrov, D.; Xing, L.; Li, W. Single-Solvent-Based Electrolyte Enabling a High-Voltage Lithium-Metal Battery with Long Cycle Life. *Adv. Energy Mater.* **2023**, *13* (30), No. 2300918.

(30) Ma, X.-X.; Shen, X.; Chen, X.; Fu, Z.-H.; Yao, N.; Zhang, R.; Zhang, Q. The Origin of Fast Lithium-Ion Transport in the Inorganic

Solid Electrolyte Interphase on Lithium Metal Anodes. *Small Struct.* **2022**, 3 (8), No. 2200071.
(31) Xie, J.; Sun, S. Y.; Chen, X.; Hou, L. P.; Li, B. Q.; Peng, H. J.; Huang, J. Q.; Zhang, X. Q.; Zhang, Q. Fluorinating the solid electrolyte interphase by rational molecular design for practical lithium-metal batteries. *Angew. Chem. Int. Ed.* **2022**, *134* (29), No. e202204776.
(32) Huang, Y.; Ji, Y.; Zhang, L.; Cai, C.; Fu, Y. Integrated Configuration Design Strategy Via Cathode-Gel Electrolyte With Forged Solid Electrolyte Interface Toward Advanced Lithium-Sulfurized Polyacrylonitrile Batteries. *Adv. Funct. Mater.* **2023**, *33* (44), No. 2306484.
(33) Prescher, C.; Prakapenka, V. B. DIOPTAS: a program for reduction of two-dimensional X-ray diffraction data and data exploration. *High Press. Res.* **2015**, *35* (3), 223−230.
(34) Juhás, P.; Davis, T.; Farrow, C. L.; Billinge, S. J. PDFgetX3: a rapid and highly automatable program for processing powder diffraction data into total scattering pair distribution functions. *J. Appl. Crystallogr.* **2013**, *46* (2), 560−566.
(35) Neese, F.; Wennmohs, F.; Becker, U.; Riplinger, C. The ORCA quantum chemistry program package. *J. Chem. Phys.* **2020**, *152* (22), No. 224108, DOI: 10.1063/5.0004608.
(36) Klamt, A.; Schüürmann, G. COSMO: a new approach to dielectric screening in solvents with explicit expressions for the screening energy and its gradient. *J. Chem. Soc., Perkin Trans.* **1993**, *5*, 799−805.
(37) Lu, T.; Chen, F. Multiwfn: A multifunctional wavefunction analyzer. *J. Comput. Chem.* **2012**, *33* (5), 580−592.

https://doi.org/10.1021/acsami.4c02326
ACS Appl. Mater. Interfaces 2024, 16, 20618−20625